Conception and optimization of an ammonia synthesis superstructure for energy storage

Christian Quintero-Masselski, Jean-François Portha, Laurent Falk

Conception and optimization of an ammonia synthesis superstructure for energy storage

Christian Quintero-Masselski [a], Jean-François Portha [a*], Laurent Falk [a]

[a] *Université de Lorraine, CNRS, LRGP, F-54000 Nancy, France*

Abstract

Ammonia has a potential as carbon-free and high-energy density compound for chemical storage of renewable energies and its synthesis from green H_2 requires to be as energetically efficient as possible. In this work, a superstructure optimization methodology for process synthesis is proposed and applied to an ammonia production process. The approach covers three different scales: process, equipment, and molecules. Process scale refers to finding the optimal process structure, while the equipment scale is related to the best set of operating conditions, and the molecular scale studies two catalysts (Fe and Ru) with their respective kinetic rates. The optimization intends to minimize the Levelized Cost of Ammonia (LCOA) and maximize the energy efficiency. The best trade-off is found with the Ru catalyst, with an LCOA of 766 €/tNH_3 and 57.2 % of energy efficiency. In comparison with reference cases, the LCOA decreases 0.6 % and the energy efficiency increases 1.5%. The main improvement is found in the pressure, 75 bar, reduced in 25 %. The production of 11.6 tNH_3/day equals to 2.5 MW of stored power from 3 MW supplied as H_2 to the process, with a total energy consumption of 10.67 kWh/kgNH_3, including prior H_2 and N_2 production processes.

Keywords: process synthesis, superstructure optimization, multiscale modelling, renewable energy, energy storage.

1. Introduction

The Global Renewable Outlook 2020 report, from the International Renewable Energy Agency (IRENA), highlighted the progress that renewable technologies have made during the last decade, with a substantial decrease in the global weighted average Levelized Cost of Energy (LCOE) for solar Photovoltaic (PV) and onshore wind projects. The former has had a reduction of 82 %, reaching 68.4 $/MWh, while the latter has dropped in 45 % to 52.8 $/MWh. Moreover, this trend is expected to continue in the next decade, with prospects of decreasing 58 % and 25 % by 2030, with an LCOE around 40 $/MWh for both technologies [1]. According to current policies, renewables sources of energy will keep playing a key role in the global share of energy in the upcoming years, boosting the energy transition and requiring strategies for the development and implementation of effective and affordable methods for a higher integration of renewables into the energetic network.

However, solar and wind sources of energy have an inherent characteristic related to intermittency, seasonality and uncertainty associated to climate, as well as the lack of a storage system, requiring the produced energy to be consumed immediately. This barrier is the main challenge to overcome, as there exists a mismatch between periods of energy production and consumption. A partial solution consists in developing efficient systems for transmission and demand response, but it is still necessary to use energy storage systems, capable of collecting the produced energy whenever possible and of making it available when required [2]. Among the energy storage alternatives, chemical storage systems are considered one of the best mechanisms in terms of adaptability to intermittencies and capacity for storing large quantities of energy, during long periods of time [3]. This type of storage involves the use of electric renewable energy to synthesize chemical compounds for their storage until energy demand increases, following with a compound decomposition to make energy available in form of electricity. In the last

* Corresponding author at: *Université de Lorraine, CNRS, LRGP, F-54000 Nancy, France*,
Tel +33 03 72 74 38 78 *E-mail address*: jean-françois.portha@univ-lorraine.fr (J.-F Portha)

years, hydrogen has gained a key role as a renewable energy carrier and research has been done in the use of hydrogen in two routes: (i) carbon chemistries, for the synthesis of fuels in Power-to-Liquids (P2L) processes such as methanol [4,5] and diesel [6], or in Power-to-Gas (P2G) technologies, for methane production [7,8], and (ii) nitrogen (N_2) carbon-free chemistries, for the synthesis of ammonia [2]. In comparison with carbon chemistries for H_2 storage, ammonia (NH_3) has an advantage in the quantity of recovered energy in chemical form. For the same basis of input energy to the synthesis of these chemicals, energy stored as NH_3 represents 55 %, while for synthetic methane equals 52 % and methanol saves around 47 %. Energy consumption losses are associated with electrolysers, accounting for almost a third of input energy, whilst for the chemical synthesis process it varies between 12% for NH_3 to 20% for methanol [9].

Ammonia, as an energy carrier, has several advantages in comparison with hydrogen. The latter is stored at least at 300 bar or at cryogenic temperatures, while NH_3 storage in liquid phase needs either a moderate refrigeration temperature of -20 °C at atmospheric pressure, or an ambient temperature for a relatively low pressure of 8.7 bar [10]. Moreover, the storage cost of pure hydrogen is 14.95 \$/kg H_2, while the same amount of H_2 contained in ammonia costs 0.54 \$/kg H_2 [11], around 4% of pure hydrogen expense. Storage energy requirements are about 11.82 kWh/kg for pure H_2 and 2.45 kWh/kg for NH_3, being 80% lower. Also, the volumetric energy density is more than twice in ammonia than in hydrogen, with 7.1 MJ/L and 2.9 MJ/L [3]. In this context, energy storage in chemical form using ammonia emerges as a potential energy carrier to overcome difficulties of renewable intermittent sources.

Ammonia is mainly produced with the Haber-Bosch (HB) process, using nitrogen and hydrogen, following the chemical reaction in Eq. (1).

$$N_2(g) + 3H_2(g) \leftrightarrow 2NH_3(g)\,, \qquad \Delta_r H^o_{298K} = -92.44\ kJ/mol \tag{1}$$

Due to N_2 triple bonding of molecules and low reactivity, a catalyst is required. Commonly, iron oxide catalysts are used due to their low investment cost, and the wide knowledge of their behaviour. Nevertheless, research on ruthenium-lanthanoids oxides [12,13], barium-promoted cobalt catalysts [14] and wüstite-based catalysts [15,16] can also be found. Being an exothermic chemical reaction, heat is produced when ammonia molecules are formed, requiring a cooling system to avoid catalyst damage and reverse reaction. Also, with the reduction in the number of moles, a displacement towards the products is favoured with high pressures. Typical operating conditions in ammonia reactors vary between 350-600 °C, and 150-300 bar [17], which require a great amount of thermal and mechanical energy. Even at these conditions, the NH_3 conversion per pass remains low (25-30 %) due to a thermodynamic constraint [18].

As the interest resides in storing renewable energy as ammonia, recent references dedicated to the synthesis of ammonia from renewable sources of energy are mentioned hereafter.

Ishaq and Dincer proposed a two-cascaded reactor configuration, to analyse the influence of pressure and temperature over the ammonia production, achieving a 61.1 % energetic efficiency (based on the Low Heating Values (LHV)), and a 65.5 % of exergetic efficiency [19]. Hasan and Dincer developed an integrated process for NH_3 and power production with wind and solar PV sources of energy, finding values for energy and exergy efficiency of 75.8% and 73.6%, resulting only from the use of wind energy, as solar PV tend to be less efficient with 18.8% and 19% of energy and exergy efficiencies [20]. Osman et al., explored the design, simulation, and optimization of an integrated NH_3 plant in a high insolation region using PV and Concentrated Solar Power (CSP). The optimized plant reached 36.3% of energetic efficiency and a levelized cost of ammonia production of 718 \$/t [21]. Demirhan et al. studied the

influence of the feedstock type for H_2 recovery, its price and availability for the synthesis of ammonia, using a global optimization framework. They integrated hardwood, corn stover and municipal solid waste, as biomass sources, with wind and solar power for water electrolysis, to find the optimal process topology, with economic and environmental analysis [10]. Zhang et al., compared the use of biomass gasification (Biomass to Ammonia, BtA), Steam Methane Reforming (SMR) (Methane to Ammonia, MtA) and water electrolysis using renewable energy (Power to Ammonia, PtA) in terms of LHV energy efficiency and of Levelized Cost of Ammonia (LCOA). Among these three scenarios, PtA had an energetic efficiency of 74%, higher than the others, 44% in BtA and 61% in MtA. However, they found the inverse relation in terms of price, as MtA costs around 400 $/t and BtA 450 $/t, while PtA costs around 544 €/t and is not currently economically feasible due to electrolysis stacks and electricity costs [22]. Armijo and Philibert studied a flexible production of hydrogen and ammonia from variable solar and wind energy in Chile and Argentina. They determined that the use of a hybridized wind-solar system can help to reduce the production cost of ammonia, as the variability of each source when used isolated increases the cost due to the need of intermediate storage of hydrogen, associated to a flexible electrolyser and a fixed ammonia unit. Moreover, they reported hydrogen prices close to and even less than 2 $/kg, which starts to compete with the 1.5 $/kg from a SMR process. Over the short term, they expect an LCOA below 500 $/kg, being competitive with the 300 – 600 $/kg value of the market [23]. Sánchez and Martin evaluated a three-reactor configuration with direct and indirect heat exchange. A higher conversion per pass was obtained in the indirect cooling configuration, with a production price of 1.35 €/kg of ammonia [24]. Yoshida et al., focused their work on comparing Fe- and Ru-based catalysts and their impact in the scale of ammonia production. For production scales near 500 t/day, the Fe-based catalyst shows the lowest cost of production at 150 bar of pressure. However, for smaller scales, around 10 t/day, the Ru-based catalyst is preferable, with a system pressure of 50 bar [25].

Most works describing a HB process using renewable energies are focused on evaluating multiple sources of energy to determine the best alternative, using economic and energetic criteria as reference. However, the ammonia synthesis structure remains unchanged, even if the efficiency of the process is highly dependent on the type of equipment used and on the setting of the operating conditions. In this context, there is an opportunity to develop strategies which allow to optimize the choice of equipment, of the catalyst, and the process structure accordingly with the operating conditions.

In the present work, a methodology for process synthesis using superstructure optimization is presented, which is applied to the case of ammonia production, using H_2 and N_2 issued from the use of wind energy. The novelty of this work resides in performing a multiscale study of a HB process architecture, involving three different scales: process, equipment, and molecules. The process scale refers to finding the optimal process structure among 15 process structure alternatives. The equipment scale is related to 10 continuous variables, such as operating conditions common to multiple units, and the search of milder conditions in comparison with industrial cases. The molecular scale studies two catalysts (Fe and Ru) with their respective kinetic rates. A global optimization is carried out, leading to the minimization of the LCOA and the maximization of the energy efficiency of the process. Particularly, this study focuses its attention on the ammonia synthesis loop structure at its connectivity level, equipment by equipment, considering upstream sections such as the recovery of raw materials from renewable energy as an already conceived process. Also, as ammonia is intended to be stored in liquid phase, its decomposition for hydrogen recovery will not be considered.

The paper is divided into the following sections: section 2 describes the superstructure optimization strategy and the materials used. Section 3 details the superstructure modelling and the mathematical formulation of the optimization problem, with the Key Performance Indicators (KPI) definition.

Subsequent section 4 treats the results and their discussion, and finally, section 5 concludes with the main findings of this work and the perspectives for the following stages.

2. Methodology and materials

2.1. Superstructure optimization strategy

Process engineers are regularly faced with the challenge of choosing the best possible structure for a material and energy conversion process. Usually, based on their own experiences and on heuristic rules, they perform a Conceptual Process Synthesis (CPS) in a limited field of research, which includes a set of foreseen unit operations, associated to equipment and operating conditions. This design is typically evaluated by economic, energetic, or environmental criteria, which allow to choose the design with the better performance. Over the years, CPS methods have been categorized according to two groups: (i) based on hierarchical decompositions, and (ii) based on superstructure synthesis, the latter being of interest in this work. Since a process needs to be conceived or improved, and several process alternatives exist to attain desired outcomes, a superstructure can be defined as the process architecture built to evaluate several process alternatives simultaneously, to find the optimal configuration in terms of equipment interconnection and operating conditions, allowing to optimize a unique or a set of objective functions. This means that instead of being a fixed process flowsheet, the superstructure has the flexibility for evaluating all existing process paths. To do so, additional units are added to the flowsheet to act as switches that divert the overall incoming mass flow towards a specific downstream section of the process, as described in Fig. 1. These switches possess as many output streams as paths to evaluate, and for each path a corresponding integer number is associated. For n outgoing paths, the optimization algorithm will dictate an i^{th} path ($i \in [1, n]$) for its evaluation.

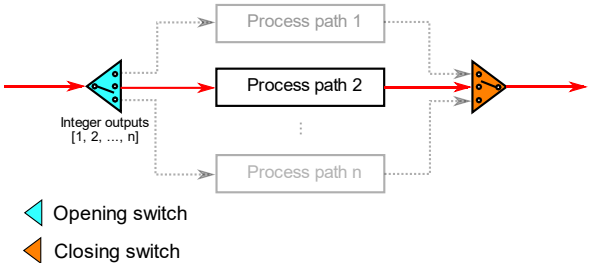

Fig. 1. Superstructure path switch.

CPS using superstructures involve three steps: (i) building the superstructure which contains the feasible structures of the process, (ii) translating the superstructure into a mathematical formulation for its optimization, and (iii) the computation of the optimization itself [26,27]. In the scope of this work, using a computational software for process modelling and simulation based on conventional equipment, imposes to focus our attention on traditional approaches for representing the process flowsheet. Steps (ii) and (iii) previously stated, will be treated in Section 3.

The State-Equipment Network (SEN) representation [28] is used in the present work as the approach for building the superstructure. It is based on the existence of material nodes, called states, and transformation nodes, known as equipment, which performs a specific task imposed by the optimization algorithm, to connect two different states. In process simulation software, these nodes can be formally represented by classic flow splitters or mixers [29]. For the sake of the reader, these nodes acting as structural switches, will hereafter be mentioned as *opening* and *closing switches*, to differentiate them from actual splitting and mixing units of the process. The main difference lies in the type of variable associated to the units, as they can be: (i) continuous, in the case of splitting and mixing units, where all

ingoing and outgoing streams contain some fraction of flowrate, or (ii) discontinuous (i.e., integer), in the case of *opening* and *closing switches*, where only one of the incoming and one of the outcoming streams possess a flowrate.

The strategy proposed in this work, consists of six steps that englobe the evaluation of a simplified superstructure. The general workflow of the superstructure conception and optimization strategy is described in Fig. 2.

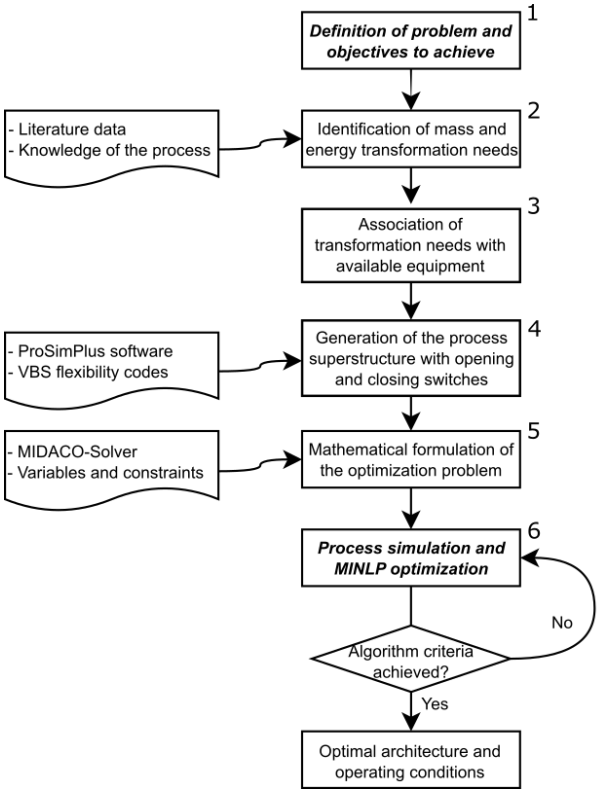

Fig. 2. Methodology structure.

Step 1 consists of defining the problem and the expected achievements with the superstructure optimization. Even if the process needs to be conceived from scratch or based on a reference case, the user must declare the limits of the system, using the input available data and the desired outcome. The optimality of the solution will be judged based on a unique or a set of KPI defined by the user. Next, step 2 is assigned to identify the mass and energy transformations required to translate raw materials into desired products. These transformations include any physical and chemical change in the initial and intermediate states of the process, such as pressure increase or decrease, heat exchanges, chemical reactions, etc. Data from the literature and the previous knowledge of the process are useful for these identifications, as they allow to announce process constraints in terms of operating condition ranges.

The use of a process simulation software limits the search of the optimal unit arrangement to the predefined models of equipment. The equipment to be evaluated is selected according to the process needs, as commonly technological or economic limitations exists. The association between transformation needs of step 2 and the available equipment is made in the step 3. Step 4 intends to translate the identified equipment and connectivity into a flowsheet in the process simulation software. *Opening* and *closing switches*, as well as any identified operating condition susceptible to be optimized, are defined by a set of scripting codes, which allow to give flexibility when different paths are to be evaluated, according to the optimization algorithm directives. Once the superstructure is defined, the

decision variables, constraints, and objective functions must be declared. The mathematical formulation of the optimization problem implies setting the algorithm parameters according to the criteria to consider a solution as optimal or not (see Appendix B). Finally, step 6 is dedicated to the iterative calculation until the criteria are achieved, with the declaration of a single or a set of solutions as optimal.

2.2. Process simulation software

In this work, the ProSimPlus steady-state simulation software of ProSim is used as a tool for the superstructure simulation [30]. The software is based on the sequential modular approach and is very helpful for defining the equipment interconnections, using Visual Basic Scripts (VBS) language. It can manage external optimization algorithms without the need of an additional interface to ensure the communication software-algorithm [31].

2.3. Optimization algorithm

Solving process engineering superstructures requires to consider continuous and discrete variables using Mixed-Integer Non-Linear Programming (MINLP) algorithms [32]. For this work, MIDACO-Solver is used, as it has proven to be useful for its integration to ProSimPlus software for other applications of superstructure optimization [29,31]. This algorithm is built as a general-purpose solver for mono- and multi-objective optimization problems, acting as a black box capable of handling non-explicit objective functions, with or without equality or inequality constraints, as well as being able to handle critical properties such as non-linearities or discontinuities. It solves multi-objective MINLP with the principles of an extended evolutionary Ant Colony Optimization (ACO), based on the gaussian probability density functions and the generation of ants/individuals [33]. For constraint handling, it includes the Oracle penalty method, which aims to find the global optimal solution with an oracle parameter which is self-adaptative [34]. The solver has been used in several applications, such as space trajectory [35], biotechnology [36], energy cycles [37] and natural gas plant optimizations [38].

An important characteristic of MINLP optimization in superstructures is the criteria used to determine whether a solution is optimal or not. MIDACO includes two types of stopping criteria: hard limit and algorithmic. The former allows the user to impose a maximal time or number of iterations. The latter remains an algorithmic decision, for which multiple options are available, for instance, achieving a certain number of evaluations without any improvement of the objective functions. Certainly, as all metaheuristic algorithms, it does not guarantee finding the optimal solution, however the exploration limits for the algorithm to find optimal points is considered sufficiently large to achieve a good trade-off between the performance indicators. The reader can find more information about the criteria in the user manual [39] and in the Appendix B.

3. Ammonia superstructure optimization

The definition of the reference cases and the scale of production is described in section 3.1. Superstructure modelling is treated in section 3.2, detailing each stage of the process, as well as the assumptions made in the flowsheet. The process considerations and hypothesis are described in section 3.3. Next, a brief description of the economic calculations is made in section 3.4, followed by the mathematical formulation of the optimization problem in section 3.5, which includes the definition of the objective functions, the set of decision variables and constraints.

3.1. Reference case and scale of production

The superstructure proposed in this work is compared with a simple reference case of an ammonia synthesis loop, for which data of iron- and ruthenium-based catalysts is found [25]. The reference

process, consisting of two compressors and two reactors is simulated to match with the hypothesis from this work, namely, economic correlations and energy efficiency calculations. Two base cases are employed, one for each catalyst: Fe at 150 bar and Ru at 100 bar. A constant inlet feed of H_2 of 45 kmol/h allows to achieve a production of around 11.6 t NH_3/day, similar to one of the process scales studied by Yoshida et al. [25]. Upstream requirements of power for H_2 production are equal to 4.2 MW, considering a specific consumption of 46.7 kWh/kg H_2 for water electrolysis [40]. Assuming a wind turbine capacity factor of 43 % [41], the nominal capacity required only for H_2 recovery is about 9.8 MW.

3.2. Superstructure modelling

The superstructure can be divided into four main stages, as seen in Fig. 3: compression, reaction, separation and recycle. In the compression and reaction stages, the intermediate opening and closing switches are included. Their objective is to bypass certain zones of the process when evaluating a specific path. Consider, for instance, the compression stages and the switches A_1 and A_2. In this case, the superstructure makes possible to evaluate 2, 3 or 4 compressors. If only two compressors are required, the switch A_1 will connect with the closing switch A. For evaluating three compressors, switch A_1 will connect to intercooler 5 and, in the same logic, switch A_2 will connect to switch A. Finally, when using four compressors, switch A_1 and A_2 will connect with intercoolers 5 and 7, respectively. More details on process paths are found in the Appendix A, while coding samples of the intermediate opening switches are available in the Supplementary Materials.

Raw materials are fed into the process in a 3:1 stoichiometric ratio of H_2:N_2, at 30 °C and 10 bar. Feed streams of raw materials are mixed and compressed with a set of compressors with intercooling stages. Gases at high temperature and pressure enter the reaction zone and the conversion takes place in catalytic reactors. The outgoing hot stream enters a separation stage where ammonia is recovered in liquid phase, while the top stream, mainly composed of H_2 and N_2, is recycled and mixed with fresh feed.

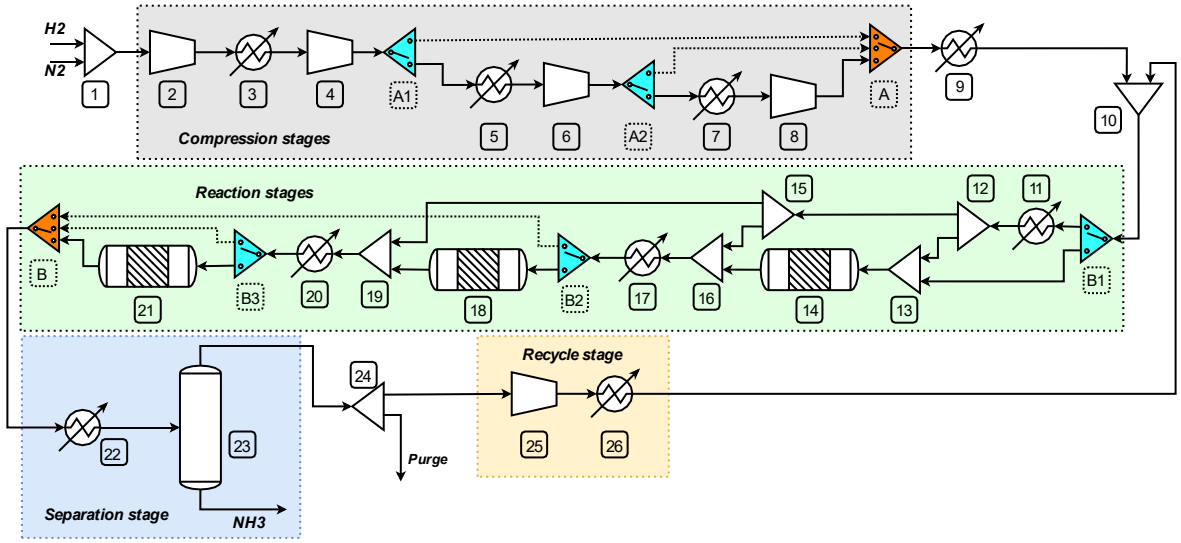

Fig. 3. Process flow diagram of the superstructure. Type of equipment: mixer (1, 10, 13, 16, 19), splitter (12, 15, 24), compressor (2, 4, 6, 8, 25), heat exchanger (3, 5, 7, 9, 11, 17, 20, 22, 26), catalytic reactor (14, 18, 21), condenser (23), opening switch (A1, A2, B1, B2, B3), closing switch (A, B).

According to Fig. 3, feed streams are mixed in unit 1 prior entering the compression stage. Given the system pressure P, the number of compressors used can vary between 2, 3 and 4, as shown by the intermediate opening switches $A_1 - A_2$ and the closing switch A. As the ammonia synthesis process

tends to use high pressure levels, using a unique compressor would require a great amount of energy, which can be reduced when using multiple compressors. Minimizing the required energy is important for this type of process of energy storage, and the following relation is used as a specification in the set of compressors:

$$r_i = {r_t}^{1/n} \tag{2}$$

The pressure ratio r_i between intermediate stages i and $i+1$ can be associated to the global pressure ratio r_t (i.e., ratio between output and input pressures of the compression zone) and the total number of stages n to minimize the required work [42]. According to the number of compressors selected, the intermediate switches A_1 and A_2 will deviate the process flow rate, and the compressors will set its outlet pressure following the relation given by Eq. (2).

The possibility of using up to three adiabatic reactors filled with Fe-based or Ru-based catalyst is included, hereafter known as Fe and Ru configurations. The length of each bed is variable, and the superficial velocity is fixed at 0.5 m/s to guarantee a low pressure drop through the reactors. The diameter is the result of calculations between the chosen length and the specified superficial velocity. The thermodynamic equilibrium limitation induces low conversions and imposes the use of multiple catalytic beds with intermediate cooling stages. Two reactor configurations are analysed: (i) Adiabatic Quench Cooling Reactor (AQCR), which uses a fraction of the feed for quenching the outgoing stream of each catalytic bed, and (ii) Adiabatic Indirect Cooling Reactor (AICR) which uses an external utility to cool down the streams coming out of the reactors [43]. For further comprehension of the reaction stage structure, a graphical comparison between the possible paths is shown in the Appendix A.

Depending on the catalyst used, a specific kinetic rate expression is considered. For the Fe catalyst, the modified Temkin-Pyzhev equation is employed [44], shown in Eq. (3), which is based on partial pressures of each constituent P_i, and includes kinetic (k_c), equilibrium (k_a), and adsorption (k_{NH3}) constants, as well as parameters α and ω. Data corresponding to each parameter where retrieved from [45].

$$r_{NH3} = \frac{k_c \cdot (P_{N2} \cdot k_a^2 \; - \; P_{NH3}^2 / P_{H2}^3)}{(1 + k_{NH3} \cdot P_{NH3} / P_{H2}^{\omega})^{2\alpha}} \tag{3}$$

On the other hand, for the Ru catalyst, Eq. (4) describes the rate expression, based of compounds activity coefficient (a_i), including kinetic (k_f), equilibrium (k_a) and adsorption (k_{H2}, k_{NH3}) constants. Constants expressions and activity coefficient correlations can be found elsewhere [25,46].

$$r_{N2} = \frac{k_f \cdot \left[{a_{N2}}^{0.5} \cdot \left(\frac{{a_{H2}}^{0.375}}{{a_{NH3}}^{0.25}} \right) - \frac{1}{k_a} \cdot \left(\frac{{a_{NH3}}^{0.75}}{{a_{H2}}^{1.125}} \right) \right]}{(1 + k_{H2} \cdot {a_{H2}}^{0.3} + k_{NH3} \cdot {a_{NH3}}^{0.2})} \tag{4}$$

Partial and global conversion are useful process metrics. As H_2 and N_2 are fed in stoichiometric proportion (3:1), the conversion of hydrogen is sufficient to describe the conversion in the system. Eq. (5) indicates the partial conversion of hydrogen in the i^{th} catalytic bed and Eq. (6) the global hydrogen conversion of the process.

$$X_{H2}^{i} = 1 - \left. \frac{\dot{F}_{H2}^{out}}{\dot{F}_{H2}^{in}} \right|_{ith\ bed} \tag{5}$$

$$X_{H2} = 1 - \left. \frac{\dot{F}_{H2}^{out}}{\dot{F}_{H2}^{in}} \right|_{process} \tag{6}$$

where $\dot{F}$ denotes the molar flow of hydrogen and superscripts in and out indicate the inlet and outlet streams of the reactor or process.

The separation of the hot stream coming from the reaction stage requires cooling and condensing the ammonia vapor phase, while nitrogen and hydrogen leave the condenser at the top gas stream. The best separation occurs at higher pressures and lower temperatures, as the hydrogen and nitrogen compounds are non-condensable, requiring only to adjust the separation temperature through the optimization.

Lastly, as a single pass through the catalytic beds is not enough to achieve high conversions, unreacted gases are recovered from the separation stage and recycled to be mixed with fresh feed. After a stream purge fixed at 1%, due to the hypothesis of absence of inert compounds, a single stage compressor and a heat exchanger (HEX) are used to ensure an isothermal and isobar mixing prior the reaction stage (module 10 in Fig. 3).

3.3. Process considerations and hypothesis

The models used for each equipment in the process flowsheet simulation are described hereafter. The process is simulated using the Predictive Peng Robinson (PPR78) thermodynamic model [47], available in ProSimPlus thermodynamic database, which allows to predict the binary interaction parameters between compounds.

Simple compressors are considered to have isentropic, mechanic, and electrical efficiencies of 75 %, 95 % and 100 %, respectively. For the compression zone, temperature fixed by the intercoolers is equal to 25 °C. A temperature limit can be fixed at the outlet stream of the compressors, to avoid dangerous levels. The outlet temperature of the compressors can exceed 200 °C in cases where 2 compressors are used at pressures higher than 150 bar. However, these extreme zones of compression imply a poor energetic efficiency and are far from being optimal, meaning that it is not necessary to impose a constraint. The compressor in the recycle stage has as specification the same outlet pressure as the outlet pressure of the compression stage. HEX consist only of one side stream, with a desired outlet temperature as specification. This simplification is made to reduce global calculation time at this stage of the study, as finding the optimal flowrate of utility fluid which allows the best recovery of energy is time consuming. A couple of case studies were carried out, in which the heat exchangers were considered to have utilities with a minimum temperature approach of 10 K, allowing to estimate a share of the heat exchangers on the process cost around 15 %. As will be further explained, the capital expenditures are around 15 % of the LCOA and the final influence of the HEX on the LCOA would be close to 2 %, which allows to avoid this calculation during the optimization. Temperature values are dictated by the optimization, except in the AQCR configuration, where the quenching stream temperature is fixed to be 50 K lower than the temperature of the first bed inlet stream, to ensure a good temperature difference when quenching the hot outlet stream of the reactor. The recycle HEX has as specification the same temperature as the first bed inlet stream. The catalytic reactors are adiabatic Plug Flow Reactors (PFR) with variable length and diameter, filled with either a Fe- or a Ru-based catalyst. Each reactor is considered as a completely independent unit, separated from the other reactors, in contrast with common industrial applications, where different catalytic sections are contained in the same reactor envelope. Density of catalysts is 3000 and 800 kg/m3, while the bed void fraction is 0.4 and the particle diameter is 0.002 m in both cases [47]. Outlet temperature cannot exceed 800 K to prevent catalyst sintering [45]. The condenser is considered adiabatic for ammonia recovery in liquid phase. Inlet pressure is dictated by system pressure and pressure losses in the catalytic beds, while the separation temperature is dictated by the optimization.

3.4. Cost estimates

The economic evaluation is based on the calculation of expenditures of the project, using as reference the Manual of Process Economic Evaluation [48], and more specifically, the *Pré-Estime* method. This method is embedded in ProSimPlus and eases the economic estimation. The investment costs consider each equipment as the sum of parts for which a base price is calculated, based on technological and sizing parameters, as well as operating conditions. For each equipment, a specific correlation exists, which is multiplied by correction, assembly, and sizing factors to obtain the assembled real price of each module. Correlations and factors for capital expenditures calculations are available in the Supplementary Materials. Operational expenditures include maintenance costs, materials consumption, miscellaneous, among others. A plant's erected costs consist of principal and secondary equipment, erection, indirect expenses, and contingencies. Assumptions for the calculation of the LCOA are summarized as follows:

- Project lifetime is equal to 20 years, with a discount rate of 8% and 8000 hours of annual operation.
- Maintenance cost of each equipment is fixed at 3% of the unassembled price.
- Electricity price of renewable energy in the European Union (EU) is equal to 43 €/MWh [9], and assuming the energy consumption of a Pressure Swing Adsorption (PSA) unit for N_2 production, with energy demand of 240 kWh/t N_2 [21], a price of 10.3 €/t N_2 is considered.
- Hydrogen price, assumed to be produced by using water electrolysis technology with renewable energy in the EU, is fixed at 3.5 €/kg H_2 [9].
- Catalyst lifetime is assumed to be of 10 years, requiring future investments. Prices are of 15.5 $/kg [45] for Fe and 321 $/kg [25] for Ru, and they are assumed as part of the CAPEX.

3.5. Mathematical optimization formulation

The multi-objective MINLP formulation is presented hereafter.

$$
\begin{array}{lll}
\text{Minimize} & f(x,y) & x \in \mathbb{R}^{n_{con}}, y \in \mathbb{Z}^{n_{int}}, n_{con}, n_{int} \in \mathbb{N} \\
\\
\text{Subject to:} & g_i(x,y) = 0 & i = 1, \dots, m_e \ \in \mathbb{N} \\
 & g_i(x,y) \geq 0 & i = m_e + 1, \dots, m \ \in \mathbb{N} \\
 & x_l \leq x \leq x_u & x_l, x_u \in \mathbb{R}^{n_{con}} \\
 & y_l \leq y \leq y_u & y_l, y_u \in \mathbb{Z}^{n_{int}}
\end{array}
$$

Where $f(x,y)$ represents the objective functions to minimize, $g_i(x,y)$ denotes the constraints of the problem, with m_e being the number of equality constraints and $m - m_e$ the number of inequality constraints. The vector x contains the continuous decision variables, with lower and upper limits denoted by x_l and x_u, while the vector y represents the integer or discrete variables, bounded between y_l and y_u. In PSE optimization problems, equality constraints are referred to mass and energy balances of the process, performed by the simulation software, while the inequality constraints are related to technical or performance limits that are defined by the user. For the multi-objective optimization, a Pareto front will be determined, which shows the set of solutions that have the best trade-off among the objective functions.

3.5.1. Objective functions

The superstructure optimization is subject to a multi-objective problem with economic and energetic performance indicators, detailed as follows.

3.5.1.1. LCOA

An annualized cost method is used for the calculation of the Levelized Cost of Ammonia, as it allows to compare capital and operational expenditures between solutions, to identify possible improvements for cost reduction, for instance, when considering different type of equipment for the same required task. It is calculated as in the Eq. (7) and consists of the Capital Expenditures (CAPEX), the Operational Expenditures (OPEX), and the total production of ammonia $\dot{m}_{NH3}$. While the OPEX and the ammonia production are defined on a yearly basis, the CAPEX involves the total investment cost of the equipment and catalyst during the project lifetime, being necessary its calculation per year. Using the annual capital charge ratio $ACCR$, as indicated in Eq. (8), allows to determine the annualized investment expenditures, based on the discount rate a and the project lifetime n.

$$LCOA = \frac{CAPEX \cdot ACCR + OPEX}{\dot{m}_{NH3}} \tag{7}$$

$$ACCR = \frac{a \cdot (1+a)^n}{(1+a)^n - 1} \tag{8}$$

Even if a unique economic objective function is used, the LCOA will also be identified as *global LCOA*, and the introduction of the concept *reduced LCOA* defines the process contribution to the *global LCOA*, which does not include the cost of raw materials H_2 and N_2. This distinction is made as the raw material contribution remains constant, independently of the solution.

3.5.1.2. Energy efficiency of the process

The energy efficiency is calculated based on the LHV and mass flowrates $\dot{m}$ of produced ammonia and supplied hydrogen, as well as the heat and work supplied to and rejected from the system [22,49], as given by Eq. (9).

$$\eta_{en} = \frac{LHV_{NH3} \cdot \dot{m}_{NH3} + \Delta\dot{W}^- + \Delta\dot{Q}^-}{LHV_{H2} \cdot \dot{m}_{H2} + \Delta\dot{W}^+ + \Delta\dot{Q}^+} \tag{9}$$

Parameters $\Delta\dot{W}$ and $\Delta\dot{Q}$ denote the net balance of mechanical and thermal power of the system, defined by Eqs. (10) and (11), while superscripts – and + refer to a net production (-) or consumption (+) of these services. As the energy balance depends on the equipment and the values of the operating conditions chosen by the optimization algorithm, this function adapts to any solution obtained.

$$\Delta\dot{W} = \left(\sum \dot{W}_{in} - \sum \dot{W}_{out}\right) \tag{10}$$

$$If\ \Delta\dot{W} > 0, then\ \Delta\dot{W}^+ = \Delta\dot{W}\ and\ \Delta\dot{W}^- = 0$$

$$If\ \Delta\dot{W} < 0, then\ \Delta\dot{W}^- = \Delta\dot{W}\ and\ \Delta\dot{W}^+ = 0$$

$$\Delta\dot{Q} = \left(\sum \dot{Q}_H - \sum \dot{Q}_C\right) \tag{11}$$

$$If\ \Delta\dot{Q} > 0, then\ \Delta\dot{Q}^+ = \Delta\dot{Q}\ and\ \Delta\dot{Q}^- = 0$$

$$If\ \Delta\dot{Q} < 0, then\ \Delta\dot{Q}^- = \Delta\dot{Q}\ and\ \Delta\dot{Q}^+ = 0$$

$$\dot{Q}_{loss} = -\Delta\dot{Q}^- \tag{12}$$

For instance, as shown in Eq. (*10*), if the mechanical power balance $\Delta\dot{W}$ is positive, the parameter $\Delta\dot{W}^+$ is considered, while $\Delta\dot{W}^-$ is equal to zero. This also applies for the thermal power balance $\Delta\dot{Q}$, for which the cooling requirements $\dot{Q}_C$ are always greater than the heating requirements $\dot{Q}_H$ in this specific process, and a complete heat integration is possible as shown in Eq. (11), justified in the Appendix C. For this phase of the work, the concept of thermal energy loss is defined by the Eq. (12),

under the hypothesis of heat rejection beyond the system boundaries without exploitation of its heat content.

3.5.2. Decision variables and constraints

H_2 conversion is dictated not only by the operational conditions, but also by the reactor geometry (i.e., length) which has an influence on the extent of reaction. Achieving higher conversions allows to increase the annual production of NH_3 and to decrease the LCOA. However, even if higher pressures favour greater conversions, either the investments costs or the energy efficiency in compressors will be compromised. Therefore, a cost-efficiency trade-off subject to optimization should include variables that influence the most the objective functions in study. Decision variables used in the superstructure optimization are shown in the **Erreur ! Source du renvoi introuvable.**.

Table 1
Continuous and discrete decision variables

Variable	Type	Stage	Process unit §	Bounds	Units
Pressure	Continuous	Compression	2, 4, 6, 8, 25	50 – 200	atm
Inlet temperature at 1st reactor	Continuous	Reaction	9, 26	606 – 736	K
Inlet temperature at 2nd reactor	Continuous	Reaction	17	606 – 736	K
Inlet temperature at 3rd reactor	Continuous	Reaction	20	606 – 736	K
Length of 1st reactor	Continuous	Reaction	14	0.5 – 6.0	m
Length of 2nd reactor	Continuous	Reaction	18	0.5 – 6.0	m
Length of 3rd reactor	Continuous	Reaction	21	0.5 – 6.0	m
Separation temperature	Continuous	Separation	22	253 - 303	K
Split ratio at first quench splitter*	Continuous	Reaction	12	0.4 – 0.8	-
Split ratio at second quench splitter*	Continuous	Reaction	15	0.4 – 0.8	-
Number of compressors	Discrete	Compression	A_1, A_2	2 – 4	-
Reactor configuration**	Discrete	Reaction	B_1, B_2, B_3	1 - 5	-

§ Process unit reference to Fig. 3

* First and second quench splitters (AQCR) are represented by modules 12 and 15 in Fig. 3.

** The reactor configuration variable unifies the number of reactors and the cooling type (# of reactors, cooling). 1 = (1, Absent); 2 = (2, AICR); 3 = (3, AICR); 4 = (2, AQCR) ; 5 = (3, AQCR).

The process pressure, which indicates the pressure at the inlet of the first reactor and at the recompression on the recycle stage, varies between 50 and 200 atm. The boundary is considerably low as the Ru-based catalyst can achieve reasonable results at pressures below 100 atm [25]. Values of temperatures at each reactor inlet stream vary between 606 and 736 K, a sufficiently large range to explore, avoiding low temperatures with slow reaction rates, and high temperatures limiting the catalyst activity [43]. Concerning the reactor length, sensitivity analysis for the different pressures and temperatures showed that limits between 0.5 and 6.0 m are enough for the chemical reaction to achieve the thermodynamic equilibrium. Similarly, the separation temperature, dependent mainly of the pressure, varies between 303 K, useful at the highest pressures, down to 253 K, where a refrigeration is necessary to recover NH_3 at lower pressures. Also, the split ratio of the quenching splitters, which indicate the fraction of the flowrate directed to the following reactor, vary between a lower value of 0.4 to avoid low flowrates, to 0.8.

Concerning the switches for structural alternatives, they are grouped into two variables. The first one indicates the *number of compressors* to be used, varying from 2 to 4, which has an influence on switches A_1 and A_2 of Fig. 3.The second concerns the *reactor configuration*, including the number of reactors and the type of cooling. Five different configurations are possible, each one associated to a position of the switch: position 1 for 1 reactor with no cooling required; positions 2 and 3 for the AICR type with 2 and 3 reactors; positions 4 and 5 for the AQCR type with 2 and 3 reactors.

Also, a total of six inequality constraints are added to the formulation to ensure the search of feasible solutions. Two performance constraints are defined, with a minimum H_2 global conversion of 95 % and a maximum LCOA of 850 €/t NH_3, even if the price remains high in comparison with reported solutions [21,22]. Three operational constraints of the maximum achievable temperature in each one of the reactors, evoked in subsection 3.3, to be lower than ≤ 800 K. One technical constraint which concerns the convergence of the recycle loop in the process is described in the Supplementary Material.

4. Results and discussion

The results presented hereafter treat in subsections 4.1 and 4.2 the reference cases, the optimal solutions from the optimization, and the comparison between them. Following, in subsection 4.3, the specific energy consumption is detailed for each one of the process services required, highlighting the effect of main process operating conditions on them. The analysis of the process structures and their influence on the KPIs is carried out in subsection 4.4, underlining the benefits and disadvantages of considering additional units in the compression and reaction stages. Next, subsection 4.5 covers the discussion of the economic share of process components.

4.1. Reference cases

Two reference scenarios were simulated, based on a simple ammonia synthesis loop structure, using two compressors, two reactors with an AICR configuration, and a condenser for ammonia separation. Fe- and Ru-based catalysts at different pressures are the main differences between the cases. The process scale is similar to the one used in the superstructure optimization, with a N_2:H_2 stoichiometric feed (1:3) equal to 60 kmol/h, allowing to produce around 11.6 t/d of NH_3. Main operating conditions and parameters used are reported in Table 2, as well as the main results. A comparison between the reference cases and the optimal solutions found with the superstructure optimization is described in the following subsection.

4.2. Objective functions trade-off

The superstructure optimization, involving 15 structural alternatives, 10 operating conditions, and two possible catalysts, were run in 2 different optimizations, one for each catalyst. The results of the two optimizations are given by the Pareto Fronts, in Fig. 4, representing the trade-off between the LCOA and the energy efficiency of the process. For the Fe case, a total of 10496 solutions were reported, from which 45.6 % are solutions respecting all the constraints (i.e., feasible solutions), and 5 Pareto points were obtained (i.e., optimal solutions). For these optimal points, production costs vary between 755 and 815 €/t_{NH3}, the energy efficiency ranges between 55.5 % and 56.8 %, and the global H_2 conversion is comprised between 94.2 % and 95.6 %. In the case of the Ru catalyst, 15728 solutions were obtained, including 43.5 % of feasible points and 10 pareto points. The LCOA ranges between 754 and 804 €/t NH_3, the energy efficiencies vary between 55.4 % and 57.7 %, and the global H_2 conversion goes from 93.4 % to 95.9 %. It is important to highlight the weight that renewable hydrogen represents in the LCOA values obtained. A simple stoichiometric calculation with the chemical reaction of Eq. (1) suggest that, considering only the prices of 3.5 €/kg H_2 and 10.3 €/t N_2, the minimum price of ammonia production is equal to 630 €/t NH_3, which is reduced to 541 €/t NH_3 and 452 €/t NH_3 if hydrogen prices of 3.0 €/kg H_2 and 2.5 €/kg H_2 were available.

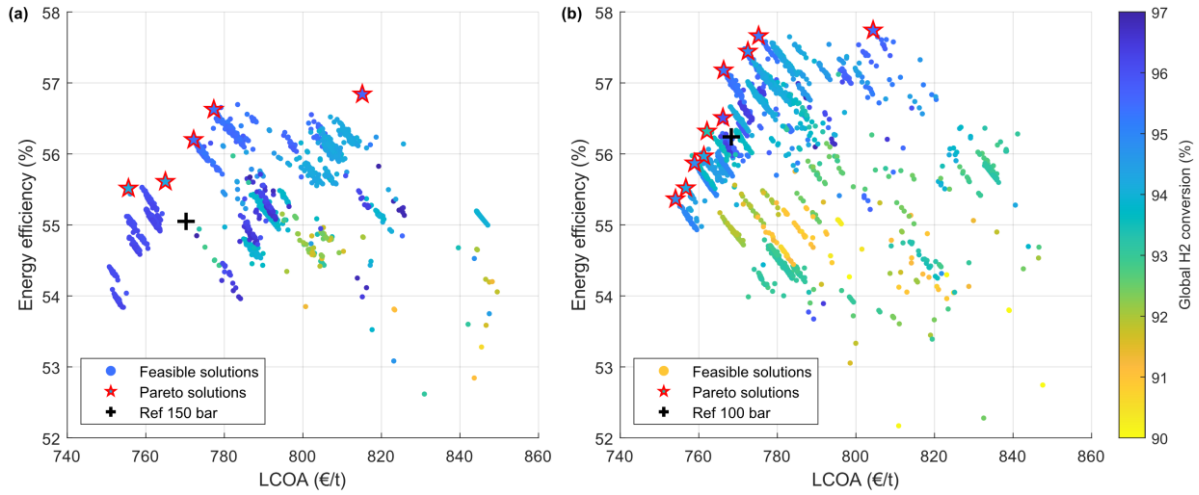

Fig. 4. Trade-off figures between the objective functions and the effect on the global H_2 conversion. (a) Fe catalyst. (b) Ru catalyst. Red stars represent the optimal solutions. Coloured points are all the feasible solutions. Black crosses represent reference cases.

The values of the KPIs and of the structural variables are presented in the Table 2 for the optimal points of both optimizations. From Fig. 4, it can be observed that price ranges are similar in both cases, although the energy efficiencies are higher for the case of the Ru catalyst. This can be justified by examining the energy efficiency objective function given by Eq. (*9*). For a constant flowrate of H_2 to the system, the energy efficiency can be improved either by reducing the amount of mechanic work supplied, by reducing the thermal energy loss or by increasing the amount of ammonia produced. The lower pressures found among the Ru case, with 38 % of solutions at values between 70 and 80 bar, give an idea of the improvement in the energy efficiency, in comparison with the most frequent pressure range found for the Fe case, being between 100 and 110 bar for 34 % of solutions. Regarding the reference points, pressures are reduced considerably, from 150 bar to around 100 bar for the Fe case, and from 100 to 75 bar for the Ru case. Concerning the structural differences between the optimal solutions, for compressors and reactors, every possible solution is obtained. However, the cooling type is either absent, in the case of only one reactor, or the AICR for the rest. In order to easily compare the optimal solutions with the reference cases, one point of each superstructure optimization is considered as optimal, being the case 3 for the Fe configuration and the case 7 for the Ru configuration, from the Table 2. Mass and energy balances for these two points are available in the Supplementary Materials.

Table 2. Results of objective functions, global hydrogen conversion, ammonia production, and main decision variables for each optimal solution of the Fe and Ru configuration. Points are organized from the less to the most expensive (LCOA). *For the reference cases, the volume of the reactors is reported.

		Fe configuration						Ru configuration										
Parameter	**Unit**	**Ref**	**1**	**2**	**3**	**4**	**5**	**Ref**	**1**	**2**	**3**	**4**	**5**	**6**	**7**	**8**	**9**	**10**
LCOA	€/t	776.95	755,58	764,98	772,18	777,32	815,13	770.90	754,07	756,71	758,91	761,29	762,09	766,14	766,33	772,50	775,22	804,37
Energy efficiency	%	54.22	55,52	55,61	56,20	56,63	56,84	56.33	55,36	55,52	55,87	55,97	56,32	56,51	57,18	57,44	57,66	57,74
Global H_2 conversion	%	95.29	94,20	94,29	95,36	95,34	95,62	96.10	94,85	94,28	94,83	94,29	93,40	95,91	95,33	94,95	95,28	95,48
Ammonia production	t/y	3884.6	3880.1	3880.2	3879.2	3874.3	3936.1	3911.6	3871,1	3839,0	3871,1	3839,0	3808,4	3911,6	3881,5	3876,0	3869,8	3887,2
Compressors	-	2	2	3	2	3	4	2	2	2	3	3	3	2	2	3	4	4
Reactors	-	2	1	1	2	2	3	2	1	1	1	1	1	2	2	2	2	3
Cooling type	-	AICR	Absent	Absent	AICR	AICR	AICR	AICR	Absent	Absent	Absent	Absent	Absent	AICR	AICR	AICR	AICR	AICR
Pressure	bar	150	98,37	98,37	98,37	98,37	93,59	100	117,53	98,37	117,53	98,37	76,98	98,37	75,84	74,57	74,44	75,54
Inlet T at 1st reactor	K	673.15	631,19	631,19	631,19	631,19	734,63	643.15	638,79	637,91	638,79	637,91	638,83	637,92	638,78	638,09	638,54	639,08
Inlet T at 2nd reactor	K	673.15	-	-	699,31	699,31	660,00	643.15	-	-	-	-	-	703,49	676,22	676,77	677,34	677,26
Inlet T at 3rd reactor	K	-	-	-	-	-	689,16	-	-	-	-	-	-	-	-	-	-	710,35
Length of 1st reactor	m	-	5,97	5,97	5,97	5,97	2,40	-	5,70	4,75	5,70	4,75	4,37	4,87	4,50	4,37	4,36	4,30
Length of 2nd reactor	m	-	-	-	2,43	2,43	5,84	-	-	-	-	-	-	1,91	2,21	2,05	2,09	2,02
Length of 3rd reactor	m	-	-	-	-	-	5,85	-	-	-	-	-	-	-	-	-	-	4,63
Separation T	K	270.45	256,51	257,53	256,51	257,53	264,06	270.45	253,46	257,53	253,46	257,53	253,64	253,00	254,55	254,70	253,99	254,42
*Volume of reactors	m^3	0.3523	-	-	0.7878	-	-	0.8797	-	-	-	-	-	-	0.8989	-	-	-

The reference and the optimal cases use 2 compressors, 2 reactors and the AICR cooling type. The main difference between them, as previously evoked, is the pressure reduction from the reference to the optimal cases, with a decrease of 35 and 25 % for Fe and Ru cases, respectively. As the pressure is reduced, the volume of the reactors tends to increase in order to achieve an equivalent conversion. Consequently, as higher operating pressures favour the condensation at milder temperatures, when the pressure is reduced, the separation temperature decreases to condense a similar flowrate of ammonia. Optimal solutions attain lower LCOAs and higher energy efficiencies, and the ammonia production has minor reductions. For the Fe case, a reduction of 0.7 % in the LCOA and a gain of 3.9 % on the energy efficiency is observed, with an NH_3 production decrease of 0.2 %. In the case of the Ru configuration, the LCOA decreased in 0.6 %, the energy efficiency increased in 1.5 %, and the ammonia flowrate had a reduction of 0.8 %. Even with the considerable reductions in pressure, equivalent results are obtained in terms of the objective functions and the amount of NH_3 produced.

4.3. Specific energy consumption

Although the energy efficiency is a valuable KPI to assess the total amount of energy recovered as ammonia, the specific energy consumption is a helpful parameter allowing to easily compare the consumption of different energy services to produce an equivalent amount of ammonia. Table 3 shows the comparison between the specific energy consumption of main process services for the reference and optimal cases.

Table 3
Specific energy consumption (kWh/kg NH_3) of the process.

Service	Reference		Optimal	
	Fe	Ru	Fe	Ru
Cooling	3.80	3.33	3.43	3.50
Heating	2.25	1.85	1.94	2.06
Net thermal energy	1.55	1.48	1.49	1.45
Water electrolysis*	8.72	8.66	8.73	8.72
Air separation*	0.20	0.20	0.20	0.20
NH_3 loop compression	0.43	0.34	0.35	0.30
Energy balance	10.90	10.68	10.77	10.67

*H_2 and N_2 production processes are considered known.

In order to have an indicator of comparison of the energy consumption of a complete NH_3 synthesis process, which includes the H_2 and N_2 production, it is considered a specific consumption of 46.7 kWh/kg H_2 for the electrolysis of water [40] and of 0.24 kWh/kg N_2 for the air separation unit [21]. Knowing the total ammonia production, it is possible to determine the consumption in kWh/kg NH_3. From Table 3, it can be observed a reduction in the net thermal energy consumption from the Fe to the Ru configuration, in both the reference and the optimal cases, with a reduction in 4.5 and 2.7 %. The water electrolysis demands less energy in the Ru reference case, as it has a slightly higher ammonia production. However, there exists a reduction on the compression energy consumption, of 20 % between the reference cases and of 14 % between the optimal cases. The process with the lowest specific energy consumption is the optimal Ru case, with 10.67 kWh/kg NH_3. For comparison, the energy requirements for the compression and recycle stages has been reported to be equal to 0.39 kWh/kg NH_3 [11]. Industrial processes of ammonia synthesis, based on natural gas, require an energy consumption of about 7.6 to 8.6 kWh/kg NH_3 [10,18,40], while most performant HB processes based on water electrolysis achieve values between 8.6 and 9.5 kWh/kg NH_3 [40]. However, this indicator is highly dependent of the type and the efficiency of the electrolyser, as it is the main driver accounting for 80 % of the energy demands.

Understanding the effect of operational conditions on the specific energy consumption is important but difficult, as there exists coupled influences among them and choosing only one parameter to evaluate the impact generated over the objective functions might mislead the analysis. It is challenging to assess the impact of an operating condition, as keeping constant the rest of variables does not guarantee being at the optimal set of conditions for the effect evaluation. To overcome this obstacle, a global analysis is preferred and discussed as follows.

4.3.1. Effect of the operating conditions on the thermal energy requirements

For the system in study, the thermal requirements are defined as the difference between hot and cold heat duties, which represents the thermal energy loss of the system, $\dot{Q}_{loss} = \sum \dot{Q}_H - \sum \dot{Q}_C$ (see Appendix C), where cooling requirements are always greater than heating requirements. Table 4 presents the thermal requirements per process stage and their share to the total, as well as the maximum temperature difference of the heat exchangers.

Table 4
Thermal energy requirements at each stage of the process, for the optimal configurations.

Process stage	Type	Fe			Ru		
		ΔT_{max} (K)	$\dot{Q}$ (kW)	%	ΔT_{max} (K)	$\dot{Q}$ (kW)	%
Compression	Cooling	157.2	77.1	4.6	136.8	66.9	3.9
Reaction	Cooling	58.7	162.1	9.8	72.9	206.3	12.1
Separation	Cooling	467.8	1421.6	85.6	459.3	1426.2	84.0
Total			1660.8			1699.4	
Reaction	Heating	170.5	84.6	9.0	198.6	98.4	9.9
Recycle	Heating	371.5	855.0	91.0	381.7	900.1	90.1
Total			939.6			998.5	
Thermal loss			721.2			700.9	

The pressures of the process, 98.4 bar for Fe and 75.8 bar for Ru, are directly reflected on the heat duties of the compression stage, being 13 % lower for the Ru case. For the reaction stage, a heating process is necessary to achieve the temperature of the first reactor inlet stream, equal to 631 K for Fe and 639 K for Ru. Evidently, as the pressure of the Ru configuration is lower, gases coming from the compression stage are at lower temperature than in the Fe case, being necessary more heat duty to achieve the reactor temperature specifications. The cooling heat duty between reactors is greater at the Ru case, as the specifications of temperature of the second reactor are 699 K for Fe and 676 K for Ru, which is directly related to the outlet temperature of first reactor, being inferred from the ΔT_{max}. The cooling down to 256.5 K for the Fe case and 254.5 K for the Ru case on the separation process requires an equivalent amount of heat duty to be extracted in both cases. However, heating in the recycle stage is 5 % higher for the Ru case in comparison with the Fe, given mainly by a greater ΔT_{max}. Even though for the Ru case, heating and cooling requirements are higher, the thermal loss given by Eq. (12) implies a better thermal integration.

Most of energy requirements are used in the separation and recycle stages. For both of the optimal solutions, as well as for the rest of the Pareto points, the separation stage represents more than 80 % of the cooling demand, while the heating power at the recycle stage stands for around 90 % of the heat requirements. Clearly, the separation method used in the process has the greatest impact over the energy efficiency of the system, as the physical separation of ammonia from unreacted gases depends on the temperature at which ammonia condensates. Requiring temperature gradients of about 460 K in the HEX at the separation stage, and of 370 K in the HEX at the recycle stage, the separation method is highly energy intensive.

4.4. Analysis of process structures

Identifying the impact of any modification in the process arrangement is important to determine whether the use of an additional unit allows to obtain a better trade-off between the KPIs. To elucidate the effect that the process structure has on the KPIs, following subsections describe the potential gains and losses when including supplementary compressors, reactors or when changing the cooling type configuration.

4.4.1. Effect of the number of compressors at different pressures

A sensitivity analysis is performed considering as reference case the point 6 of the Ru configuration, reported in the Table 2. Main parameters considered constant are the following: inlet temperature of 637.9 K and length of 4.87 m for the first reactor; inlet temperature of 703.5 K and length of 1.91 m for the second reactor; separation temperature of 253 K and the use of two compressors and the AICR cooling type. Reported KPIs are an LCOA of 766.1 €/t_{NH3} and 56.51% of energy efficiency. The effect of considering additional units of compression on the objective functions is described for three different levels of pressure. For an equal operating pressure, the number of compressors does not affect the hydrogen conversion nor the ammonia production, however it affects the economic KPI through the investment, maintenance, and electricity consumption costs, while the effect over the energetic KPI affects the overall mechanic work and thermal requirements of the process. The addition of 1 and 2 supplementary compressors at pressures of 74.4, 98.4 and 117.5 atm is carried out, as shown in Fig. 5 (a).

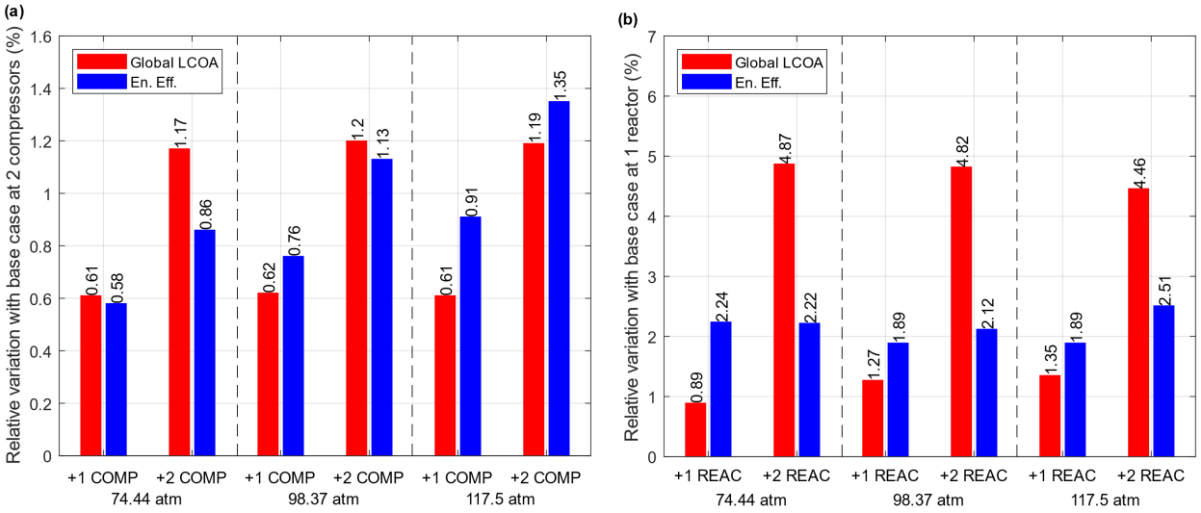

Fig. 5. (a) Relative variation of the KPIs with respect of the KPIs reported in the Case 6 for the Ru configuration, which uses 2 compressors. Effect of the addition of 1 and 2 supplementary compressors for three different levels of pressure. (b) Relative variation of the KPIs with respect of the KPIs reported in the Case 10 for the Ru configuration, when using 1 reactor. Effect of the addition of 1 and 2 supplementary reactors for three different levels of pressure.

The use of an additional unit, (+1 COMP), shows an almost equal effect on both KPIs at the lowest pressure (74.4 atm). Nevertheless, when increasing the pressure, the gain on the energy efficiency is higher than the increase of the LCOA which is induced mainly by the investment cost of the unit. On the other hand, considering two additional compressors, (+2 COMP), is only interesting at the pressure of 117.5 atm or higher, as the gain the energy efficiency is slightly higher than the increase of the LCOA. In other words, for the synthesis loop of ammonia with the Ru configuration at pressures near 75 atm, the use of only two compressors shows a good trade-off between the KPIs, while using a third compressor (+1 COMP) can be justified for the pressures of 98 and 117 atm.

4.4.2. Effect of the number of catalytic beds at different pressures

Analogously to the compressors, a sensitivity analysis is performed to understand the effect that the number of reactors has on the KPIs. The case 10 of the Ru configuration, reported in the Table 2, is considered as the base case as it has optimized length and inlet temperature for the three reactors. Parameters kept constant are the following: lengths of reactors of 4.30, 2.02 and 4.63 m, and inlet temperatures of reactors equal to 639.1, 677.3 and 710.4 K, as well as a separation temperature of 254.4 K. The same variations in pressure are carried out, while changing the number of reactors between 1, 2 or 3 units. In contrast with the compressors, the use of an additional reactor favours the reaction extension and the global conversion of hydrogen, also having an effect on the total ammonia production. However, it also has an impact on the pressure drop across the reaction stages, being necessary supplementary mechanical work for recompression at the recycle stage. Fig. 5 (b) shows the relative variation of the global LCOA and the energy efficiency with respect to the case 10 of the Ru configuration, when using only 1 reactor.

As seen in Fig. 5 (b), the use of a second reactor (+1 REAC) has a greater effect on the energy efficiency of the system, mainly induced by a higher ammonia production, while the global LCOA grows at a lower rate. Although, using a third reactor has a negative impact, as the economic KPI increases up to twice the improvement of the energetic KPI. This can be justified when comparing the contribution that the third reactor has on the ammonia production with the economic KPI, as shown in Table 5.

Table 5
Relative variation of main indicators of the sensitivity analysis for the Ru configuration, when adding one or two supplementary reactors at three levels of pressure.

Parameters	P = 75.54 atm			P = 98.37 atm			P = 117.53 atm		
	1 REAC	+1 (%)	+2 (%)	1 REAC	+1 (%)	+2 (%)	1 REAC	+1 (%)	+2 (%)
LCOA (€/t)	770.58	+ 0.89	+ 4.87	765.54	+ 1.27	+ 4.82	766.29	+ 1.35	+ 4.46
Energy Eff. (%)	56.20	+ 2.24	+ 2.22	56.07	+ 1.89	+ 2.12	55.70	+ 1.89	+ 2.51
Global XH_2 (%)	93.46	+ 1.89	+ 2.27	94.35	+ 1.63	+ 2.18	94.72	+ 1.52	+ 2.16
Mech. work (kW)	135.84	+ 0.23	+ 2.68	153.66	+ 0.16	+ 1.69	166.18	+ 0.14	+ 1.29
Energy loss (kW)	680.17	+ 1.56	+ 2.15	702.08	+ 1.28	+ 1.83	715.00	+ 1.28	+ 2.05
NH_3 prod. (t/y)	3800.34	+ 2.06	+ 2.18	3845.72	+ 1.65	+ 2.03	3855.41	+ 1.71	+ 2.43

For the three levels of pressure, using a second reactor (+1) improves more the ammonia total production than the increase in mechanical work and the thermal energy losses, which translates into a higher increase of the energy efficiency than the LCOA. However, the effect that a third reactor (+2) has on the ammonia production cannot offset the increase in the LCOA due to the investment costs. Then, for any pressure of the previously considered, the use of a second reactor (+1) allows to improve the process performance, while the use of a third one (+2) causes a detriment of the economic KPI with not much improvement of the energy efficiency.

4.4.3. Effect of the cooling type

In the reported solutions of the Table 2, a dominance of the AICR configuration over the AQCR is observed. As seen in Fig. 6, which highlights the type of reactor configuration for the feasible solutions, a distribution depending on the number of reactors and cooling type exists. For both cases, the use of two reactors with the AICR type shows a good trade-off between the KPIs, more visible for the Ru case. In comparison with the AICR, using the same number of reactors with the AQCR configuration translates into a displacement of the solutions towards a more expensive and less efficient region. The analysis of two points of the Fe case, with different cooling type, but similar number of compressors

and reactors, gives the following results: with respect to the AICR, in the AQCR the global conversion of hydrogen and the ammonia production are reduced in 1.6 %, with thermal energy losses and mechanical energy at similar levels. This is mainly due to a lower conversion per pass in the AQCR, as the cooling performed through quenching with a stream at different conditions does not guarantee an equal extent of reaction in the next reactor. The decrease in the ammonia production has a negative effect in both objective functions, as lower flowrate induces a higher LCOA (+1.8 %) and a lower energy efficiency (-2.7 %), which corresponds with the behaviour seen in Fig. 6.

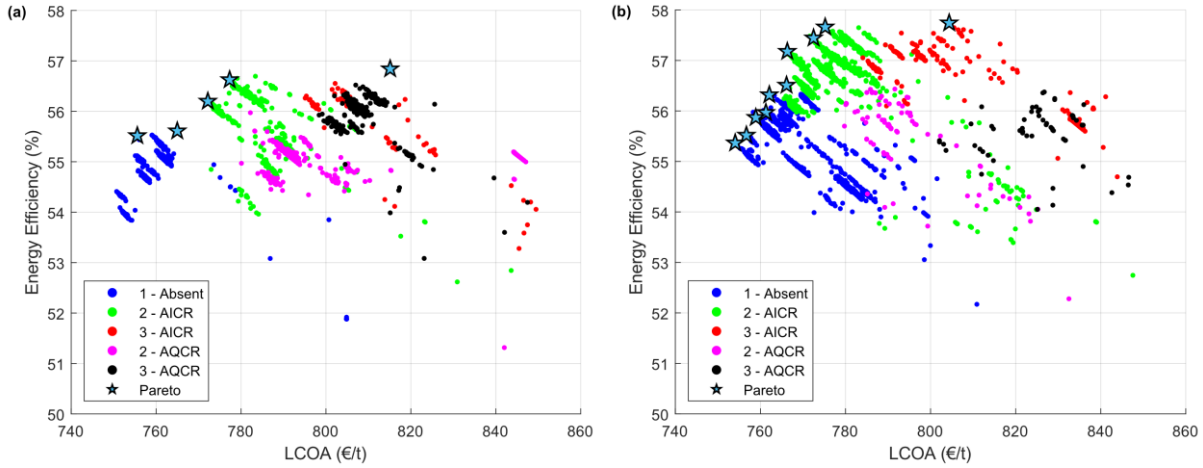

Fig. 6. Distribution of reactor configurations from all the feasible solutions. (a) Fe case, (b) Ru case. The number of reactors vary from 1 to 3, while the cooling configuration can be absent, indirect (AICR) or quench (AQCR).

Besides, the comparison between the AICR and the AQCR configurations from literature indicates that the former allows obtaining a higher conversion output and a higher ammonia production than the latter [43].

4.5. Economic criteria

The LCOA considers the sum of capital and operational expenditures, including equipment, raw materials, catalysts, and electricity. For processes using renewable sources of energy, raw materials tend to be expensive when compared to conventional fossil fuel-based processes. For instance, the H_2 cost of 3.5 €/kg translates into a share in the total OPEX of around 95 %, while the remaining includes N_2, electricity and maintenance costs. Moreover, the contribution of H_2 cost to the *global LCOA* varies from 79 % to 85 %. The *global LCOA* results then in a fixed part of raw materials, while process cost is the remaining, around 20 %, which is subject to the optimization procedure. In any case, trying to find the best suitable structure which minimizes the production cost contributes to finding the best solution, although the high cost of raw materials creates an economic barrier when trying to implement processes based on renewable energies. Table 6 details the contribution of previously evoked expenditures on the capital and operational costs for the two optimal solutions of Fe and Ru configurations.

Table 6
Annualized capital and operational expenditures and share of each type of component of the process, for the two optimal cases of Fe and Ru. %* denotes the share of the *reduced* OPEX, which excludes H_2 and N_2 costs.

Component	Fe					Ru				
	CAPEX		OPEX			CAPEX		OPEX		
	€/y	%	€/y	%	%*	€/y	%	€/y	%	%*
Catalysts	5 459	1.4	-	-	-	28 504	8.1	-	-	-
Separator	5 840	1.5	534	~ 0	0.7	4 964	1.4	453	~ 0	0.7
Compressors	145 475	37.8	14 077	0.5	18.2	116 480	32.9	11 275	0.4	16.3
Reactors	228 182	59.3	7 468	0.3	9.6	203 429	57.6	6 658	0.3	9.7
Hydrogen	-	-	2 540 009	95.8	-	-	-	2 540 009	96.1	-
Nitrogen	-	-	34 692	1.3	-	-	-	34 692	1.3	-
Electricity	-	-	55 391	2.1	71.5	-	-	50 585	1.9	73.3

In terms of capital expenditures, the main difference between the optimal points resides in the catalyst used, as the Ru-based catalyst is more expensive than the Fe-based, which translates into an increase from 1.4 to 8.1 % of the share of CAPEX. However, due to the reduction of pressure from the Fe to the Ru configuration, prices of the separation column, the compressors and the reactors decrease, as they depend on the operating pressure, among other parameters. This decrease in pressure also means less maintenance and electricity costs. The reactors stand as the most expensive equipment, which goes along with the discussion of subsection 4.4.2. Concerning the *global* operational expenditures, the high H_2 cost hides the contribution of the rest of components. When analysing the *reduced* OPEX, electricity accounts for more than 70 % of the share, being the rest the maintenance of equipment.

5. Conclusions

A methodology for superstructure optimization applied to an ammonia synthesis process was presented. The process structural alternatives included the choice of the number of compressors, number of reactors, type of cooling and type of catalyst used. The minimization of the LCOA and the maximization of the energy efficiency allowed to obtain a total of 15 optimal solutions, with values of LCOA between 754 and 815 €/t NH_3, and energy efficiencies near to 58 %. From the analysis of the process structure, the best trade-off between cost and energy efficiency was found for the solutions using 2 compressors, 2 reactors and the AICR configuration, for systems using an operating pressure below 100 bar. The Ru-based catalyst has a better performance when compared to the Fe-based, as it achieved an equivalent H_2 global conversion and ammonia production, with an operating pressure 23% lower. The daily production of ammonia of around 11.6 tonnes, with a purity above 99.6 %, translates into a total amount of 2.51 MW in chemical form as NH_3, produced from 3.02 MW supplied by the H_2, for which 4.2 MW are considered to be necessary in the electrolysis process. The analysis of the specific energy consumption allowed to find a total energy requirement of 10.67 kWh/kg NH_3 in the best of the cases, for which 80 % corresponds to the water electrolysis process and around 17 % are related to the synthesis loop.

The structural analysis of the reported solutions allowed to determine that the cooling type is dominated by processes using AICR configurations, as the AQCR showed to be more expensive and less efficient. The global optimization allows finding milder pressures, with the lowest level found with the Ru catalyst at 75.84 bar, being relatively low in comparison with industrial levels, ranging between 150 and 250 bar [10,18]. This shows the importance on developing new catalytic materials and assessing their effect on industrial processes. However, lower pressures require lower separation temperatures, as the obtained in the solution near 253 K. This implies that the condensation of NH_3 remains the most energy intensive section of the process.

The economic evaluation of the process suggests that the most expensive unit included in the process is the reactor and using a third reactor does not guarantee an improvement of the KPIs. Even if the process is optimized in terms of structure and operating conditions, the global LCOA remains high due to the cost of hydrogen issued from renewable sources (3.5 €/kg), representing around 80 % of the ammonia production cost, while the process cost share accounts for the remaining 20 %.

This methodology is a tool that can be easily exploited by engineers, needing only basic scripting codes, mainly for the switch's configuration. It can be applied in the retrofitting of industrial processes to determine whether a new technology or equipment would improve the environmental and energy performance without prejudice of the economics. Also, as multiple processes can be included in the same superstructure, it is possible to evaluate and determine the required improvements of a specific equipment or technology that will allow it to be, at least, as competitive as other technologies.

The following steps of this work include the proposal of a heat exchanger network that minimizes the utility requirements, and the HEX investment costs. Also, the evaluation of alternative types of reactors, such as the multitube and autothermal, and other types of separation equipment, such as membranes, could allow to overcome the high energy consumption associated to the separation by condensation. Finally, hybrid equipment, such as membrane reactors, can lead to smaller operating units as it allows to couple mass and heat transfer, while improving the extent of the chemical reaction, favouring not only the reduction on investment costs, but also the improvement of the energy efficiency of the process.

Nomenclature

Abbreviations

ACO	Ant colony optimization
AICR	Adiabatic indirect cooling reactor
AQCR	Adiabatic quench cooling reactor
BtA	Biomass to ammonia
CAPEX	Capital expenditures
CPS	Conceptual process synthesis
CSP	Concentrated solar power
EU	European Union
HB	Haber-Bosch
HEX	Heat exchanger
IRENA	International Renewable Energy Agency
KPI	Key Performance Indicator
LCOA	Levelized cost of ammonia
LCOE	Levelized cost of energy
LPG	Liquified petroleum gas
LHV	Low heating value
MINLP	Mixed-integer non-linear programming
MtA	Methane to ammonia
OPEX	Operational expenditures
PFR	Plug flow reactor
PSA	Pressure swing adsorption
PPR78	Predictive Peng-Robinson 78
P2L	Power to liquids
P2G	Power to gas
PtA	Power to ammonia
PV	Photovoltaic
SEN	State-equipment network
SMR	Steam methane reforming
VBS	Visual basic script

Greek symbols

α	Reaction rate parameter
$\Delta_r H_{298}$	Standard enthalpy of reaction
$\Delta\dot{E}$	Net power
$\Delta\dot{Q}$	Net thermal power
$\Delta\dot{W}$	Net mechanical work
η_{en}	Energy efficiency
ω	Reaction rate parameter

Mathematical symbols

k_{NH3}	Adsorption constant (ammonia)
k_{H2}	Adsorption constant (hydrogen)
X	Conversion

f_d	Cumulative discount factor
a	Discount rate or activity coefficient
k_a	Equilibrium constant
€	Euro
g_i	i^{th} constraint
f_i	i^{th} objective function
k_c	Kinetic constant
k_f	Kinetic constant
x_l	Lower bound
$\dot{m}$	Mass flowrate, kg h^{-1}
$\dot{F}$	Molar flowrate, kmol h^{-1}
P_i	Partial pressure of compound I, atm or bar
r	Pressure ratio
n	Project lifetime or number of compression stages
r_{NH3}	Reaction rate of ammonia
r_{N2}	Reaction rate of nitrogen
$\dot{Q}$	Thermal power, kW
m	Total number of constraints
m_e	Total number of equality constraints
$	United States dollar
x_u	Upper bound

Superscripts

-	Produced or rejected
+	Consumed
in	Inlet stream of the equipment or process
out	Outlet stream of the equipment or process

Subscripts

C	cold thermal requirements
H	hot thermal requirements
i	i^{th} position or compound
loss	Rejected or lost
t	total

Appendix

A. Superstructure building

The use of a process simulation software for superstructure optimization implies reducing the calculation time as much as possible, as it tends to be a strong time consumer. A strategy for flowsheet simplification and avoiding extra calculations in repetitive modules can be seen in Fig. A.1. It represents a multistage compression where 3 configurations need to be evaluated, with 2, 3 or 4 compressors. Instead of building the superstructure as the Type A (i.e., 9 compressors and 7 intercoolers), one could think of introducing intermediate opening switches, which allow to group together common equipment of multiple process paths, as the Type B (i.e., 4 compressors and 4 intercoolers). Ideally, intermediate opening switches should deviate all the incoming flow to a unique outlet stream, imposing zero flowrates towards the rest. However, in process simulation software a null flow would induce a calculation error in most of the modules [31], being necessary to divert at least a very small fraction to all the outlet streams. In this work, distribution ratios of the order of 10^{-9} are used to guarantee a correct superstructure calculation, while imposing non-changes in process streams that are evaluated in undesired paths (e.g., outlet pressure equal to inlet pressure in an unused compressor).

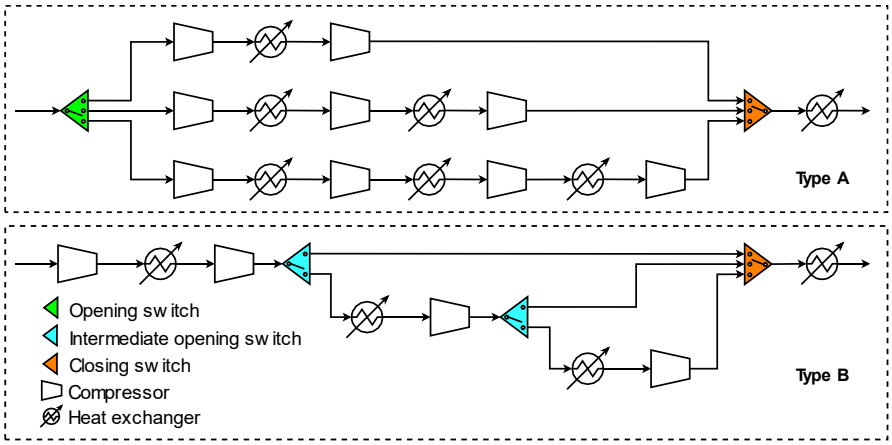

Fig. A.1. Multi-stage of compression with intercoolers.

Fig. A.2 compares the different possible paths for a section of the reaction stage. Cooling type AICR and AQCR, as well as two catalytic beds are represented. Black and red solid lines indicate used modules and streams, while grey dotted lines show non-considered modules and streams.

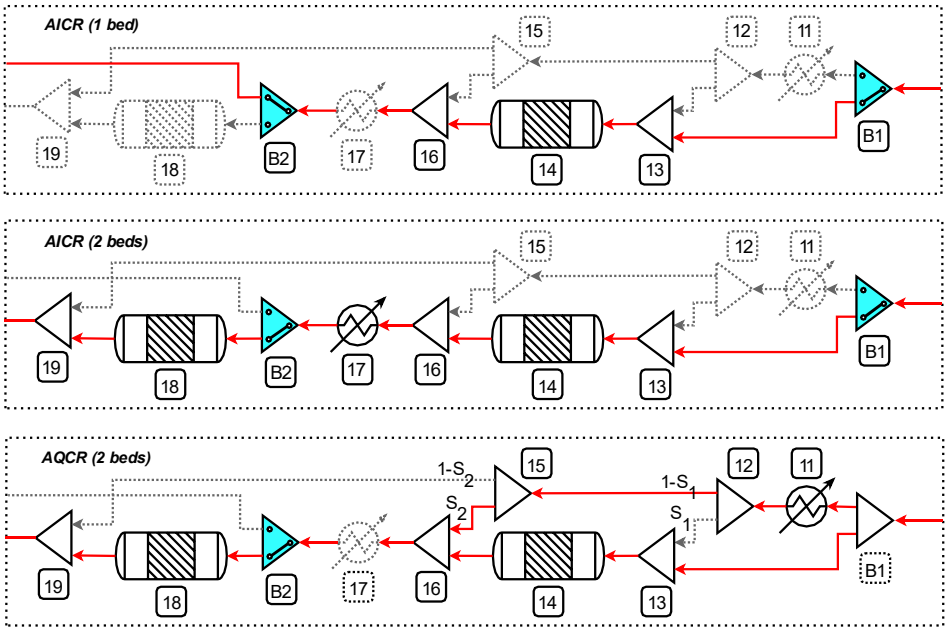

Fig. A.2. Graphical path comparison in the reaction stage. Type of equipment: HEX (11, 17), PFR (14, 18), mixer (13, 16, 19), splitter (12, 15), opening switch (B1, B2).

Note that for the AICR with 1 bed, the HEX module (17) is not used, as it is only used when the succeeding PFR is chosen, as in the case of the AICR with 2 beds. Any further heat exchange will be performed in the separation stage. In the case of using the AQCR with 2 or 3 beds, splitting ratios S_1 (splitter 12) and S_2 (splitter 15) are defined for the quenching streams.

B. Algorithm stopping criteria

The optimization algorithm permits to define one or multiple criteria, based on predefined parameters, to stop the optimization and consider the most recent optimal solution as the final single or set of optimal points. Parameters used are: (i) MAXEVAL, defined as the maximum number of evaluations that the algorithm can perform before stopping, set to 100.000, and (ii) EVALSTOP, being the maximum number of evaluations that the algorithm can perform without any improvement of the best current solution, set to 10.000. The best single or set of solutions will be judged optimal when any of these parameters is attained. Values set to these parameters are considered sufficiently large to allow the algorithm to carry out a wide search of solutions. For more information about algorithm parameters, see reference [39].

C. Energy efficiency definition

Considering the system in Fig. C.1, the associated energy balance is defined when considering any material or energy stream crossing its border. In this case, the inlet hydrogen stream ($\dot{m}_{in}$), acting as fuel for the system, and the outlet ammonia stream ($\dot{m}_{out}$) recovered as the main interest of the process, are referred as the process material streams, linked with its energy content. Supplied mechanical work includes any required compression work ($\dot{W}_{in}$), while produced mechanical work refers to turbine equipment able to recover mechanical work from the system ($\dot{W}_{out}$). Concerning the thermal power requirements, either a net heat power is supplied ($\dot{Q}_{in}$), produced ($\dot{Q}_{out}$), or even rejected ($\dot{Q}_{loss}$) from the system to its surroundings.

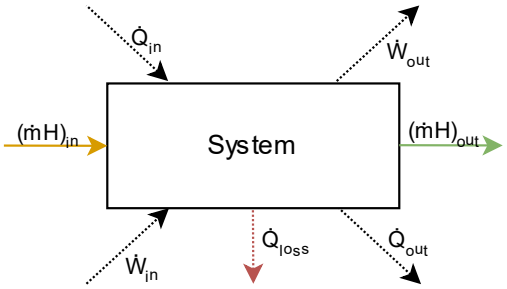

Fig. C.1. System boundaries for the energy balance

The general definition of the energy efficiency objective function is given by Eq. (C.1), as follows:

$$\eta_{energy} = \frac{(\dot{m}_{NH3} \cdot LHV_{NH3}) + \Delta\dot{W}^{-} + \Delta\dot{Q}^{-}}{(\dot{m}_{H2} \cdot LHV_{H2}) + \Delta\dot{W}^{+} + \Delta\dot{Q}^{+}} \tag{C.1}$$

where, η_{energy} represents the energy efficiency of the system, $\dot{m}$ is the mass flowrate, LHV indicates the energy content given by the low heating value, $\Delta\dot{W}^{-}$ and $\Delta\dot{W}^{+}$ are the net produced and supplied mechanical work, and $\Delta\dot{Q}^{-}$ and ΔQ^{+} represent the net produced (or lost) and supplied thermal energy. As the system is flexible to different flowsheet structures and the interest remains in a global balance of energy, only the produced or supplied term of the energy efficiency definition are used, as defined by Eqs. (C.2) and (C.3).

$$\Delta\dot{W} = \left(\sum \dot{W}_{in} - \sum \dot{W}_{out}\right) \tag{C.2}$$

$$If\ \Delta\dot{W} > 0, then\ \Delta\dot{W}^{+} = \Delta\dot{W}\ and\ \Delta\dot{W}^{-} = 0$$

$$If\ \Delta\dot{W} < 0, then\ \Delta\dot{W}^{-} = \Delta\dot{W}\ and\ \Delta\dot{W}^{+} = 0$$

$$\Delta\dot{Q} = \left(\sum \dot{Q}_{H} - \sum \dot{Q}_{C}\right) \tag{C.3}$$

$$If\ \Delta\dot{Q} > 0, then\ \Delta\dot{Q}^{+} = \Delta\dot{Q}\ and\ \Delta\dot{Q}^{-} = 0$$

$$\Delta\dot{Q} = \Delta\dot{Q}^{-}\ if\ \Delta\dot{Q} < 0, then\ \Delta\dot{Q}^{+} = 0$$

The balance of mechanical and thermal energy will then define the terms to be used in Eq. (C.1). For the process in study, mechanical work is only referred to consumed work by the compressors, as no turbines exist, and the sum of produced work is equal to zero in Eq. (C.2). Concerning the thermal energy balance, Eq. (C.3) can be used when considering that a heat exchange occurs between process streams, as the heat requirement of cold streams can be satisfied with the thermal energy available in hot streams, requiring to be cooled. Even if the procedure conceived does not include a real HEX network analysis, first results of simulations allowed to justify the use of Eq. (C.3) with a simple pinch analysis of process streams of the used HEX. Using the results of a single Pareto solution given by the algorithm in the first optimizations, the hot and cold composite curves are built, as seen in Fig. C.2, based on data of Table C.1.

Table C.1.
Data from heat exchangers for the Pinch analysis.

HEX	Type	ṁ (kg/h)	Q̇ (kW)	T_{in} (°C)	T_{out} (°C)
3	Cooling	510.92	48.41	128.90	29.72
5	Cooling	510.92	48.88	129.09	29.72
9	Heating	510.92	116.73	129.44	364.76
17	Cooling	3011.4	161.73	486.91	430.34
22	Cooling	3011.4	1473.7	455.03	-15.62
26	Heating	2499.7	902.65	-12.56	364.76

All the reported solutions have the same behaviour, with the cooling needs (hot curve) being around twice the heating needs (cold curve). This allows to suggest a possible heat integration to fulfil all the heat demands, while being necessary the use of two cold utilities, one at low temperature (near ambient conditions) and the other at high temperature.

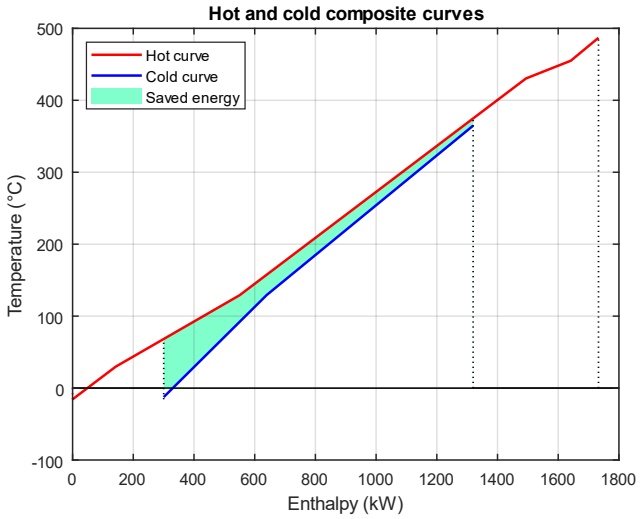

Fig. C.2. Hot and cold composite curves of a Pareto solution, with a ΔT_{min} equal to 10 K.

Considering the Eq. (C.3), the thermal supply to the system ($\dot{Q}_{in}$) is related to the hot requirements (cold curve) and the production ($\dot{Q}_{out}$) or rejection ($\dot{Q}_{loss}$) of thermal energy is associated with the cooling requirements (hot curve). With the thermal integration proposed previously, the difference between hot and cold requirements will lead to a negative heat duty. Remaining cooling needs must be satisfied with cold utilities and assuming that the heat rejected from the system is not valorised, the thermal energy balance of Eq. (C.3) will be equal to the heat loss ($\dot{Q}_{loss}$) of the system. As a result, the generalized energy efficiency of Eq. (C.1) can be simplified into the expression of Eq. (C.4).

$$\eta_{energy} = \frac{(\dot{m}_{NH3} \cdot LHV_{NH3}) - \dot{Q}_{loss}}{(\dot{m}_{H2} \cdot LHV_{H2}) + \sum \dot{W}_c} \tag{C.4}$$

References

[1] IRENA. Global Renewables Outlook: Energy transformation 2050. 2020.

[2] Ikäheimo J, Kiviluoma J, Weiss R, Holttinen H. Power-to-ammonia in future North European 100 % renewable power and heat system. Int J Hydrogen Energy 2018;43:17295–308. https://doi.org/10.1016/j.ijhydene.2018.06.121.

[3] Valera-Medina A, Xiao H, Owen-Jones M, David WIF, Bowen PJ. Ammonia for power. Prog Energy Combust Sci 2018;69:63–102. https://doi.org/10.1016/j.pecs.2018.07.001.

[4] Lonis F, Tola V, Cau G. Assessment of integrated energy systems for the production and use of renewable methanol by water electrolysis and CO2 hydrogenation. Fuel 2021;285:119160. https://doi.org/10.1016/j.fuel.2020.119160.

[5] Rafiee A. Modelling and optimization of methanol synthesis from hydrogen and CO2. J Environ Chem Eng 2020;8:104314. https://doi.org/10.1016/j.jece.2020.104314.

[6] Samavati M, Martin A, Nemanova V, Santarelli M. Integration of solid oxide electrolyser, entrained gasification, and Fischer-Tropsch process for synthetic diesel production: Thermodynamic analysis. Int J Hydrogen Energy 2018;43:4785–803. https://doi.org/10.1016/j.ijhydene.2018.01.138.

[7] Bassano C, Deiana P, Lietti L, Visconti CG. P2G movable modular plant operation on synthetic methane production from CO2 and hydrogen from renewables sources. Fuel 2019;253:1071–9. https://doi.org/10.1016/j.fuel.2019.05.074.

[8] Hidalgo D, Martín-Marroquín JM. Power-to-methane, coupling CO2 capture with fuel production: An overview. Renew Sustain Energy Rev 2020;132:110057. https://doi.org/10.1016/j.rser.2020.110057.

[9] International Energy Agency (IEA). The future of hydrogen fuel. Paris: 2019. https://doi.org/https://www.iea.org/reports/the-future-of-hydrogen.

[10] Demirhan CD, Tso WW, Powell JB, Pistikopoulos EN. Sustainable ammonia production through process synthesis and global optimization. AIChE J 2019;65. https://doi.org/10.1002/aic.16498.

[11] Bartels JR. A feasibility study of implementing an Ammonia Economy. Iowa State University, 2008. https://doi.org/10.31274/etd-180810-1374.

[12] Miyahara S ichiro, Sato K, Kawano Y, Imamura K, Ogura Y, Tsujimaru K, et al. Ammonia synthesis over lanthanoid oxide–supported ruthenium catalysts. Catal Today 2020:2–5. https://doi.org/10.1016/j.cattod.2020.08.031.

[13] Javaid R, Aoki Y, Nanba T. Highly efficient Ru/MgO–Er2O3 catalysts for ammonia synthesis. J Phys Chem Solids 2020;146:109570. https://doi.org/10.1016/j.jpcs.2020.109570.

[14] Ronduda H, Zybert M, Patkowski W, Tarka A, Ostrowski A, Raróg-Pilecka W. Kinetic studies of ammonia synthesis over a barium-promoted cobalt catalyst supported on magnesium–lanthanum mixed oxide. J Taiwan Inst Chem Eng 2020;114:241–8. https://doi.org/10.1016/j.jtice.2020.09.020.

[15] Lendzion-Bieluń Z, Jurkowski A. Surface properties of wustite based iron-cobalt catalysts for ammonia synthesis reaction. Catal Commun 2020;136:105907. https://doi.org/10.1016/j.catcom.2019.105907.

[16] Liu H, Han W, Huo C, Cen Y. Development and application of wüstite-based ammonia synthesis catalysts. Catal Today 2019;355:110–27. https://doi.org/10.1016/j.cattod.2019.10.031.

[17] Aziz M, Oda T, Morihara A, Kashiwagi T. Combined nitrogen production, ammonia synthesis, and power generation for efficient hydrogen storage. Energy Procedia 2017;143:674–9. https://doi.org/10.1016/j.egypro.2017.12.745.

[18] Appl M. Ammonia : principles and industrial practice. Weinheim, New York, Chichester,

Brisbane, Singapore, Toronto: Wiley-VCH; 1999.

[19] Ishaq H, Dincer I. Design and simulation of a new cascaded ammonia synthesis system driven by renewables. Sustain Energy Technol Assessments 2020;40:100725. https://doi.org/10.1016/j.seta.2020.100725.

[20] Hasan A, Dincer I. Development of an integrated wind and PV system for ammonia and power production for a sustainable community. J Clean Prod 2019;231:1515–25. https://doi.org/10.1016/j.jclepro.2019.05.110.

[21] Osman O, Sgouridis S, Sleptchenko A. Scaling the production of renewable ammonia: A techno-economic optimization applied in regions with high insolation. J Clean Prod 2020;271:121627. https://doi.org/10.1016/j.jclepro.2020.121627.

[22] Zhang H, Wang L, Van herle J, Maréchal F, Desideri U. Techno-economic comparison of green ammonia production processes. Appl Energy 2020;259:114135. https://doi.org/10.1016/j.apenergy.2019.114135.

[23] Armijo J, Philibert C. Flexible production of green hydrogen and ammonia from variable solar and wind energy: Case study of Chile and Argentina. Int J Hydrogen Energy 2020;45:1541–58. https://doi.org/10.1016/j.ijhydene.2019.11.028.

[24] Sánchez A, Martín M. Optimal renewable production of ammonia from water and air. J Clean Prod 2018;178:325–42. https://doi.org/10.1016/j.jclepro.2017.12.279.

[25] Yoshida M, Ogawa T, Imamura Y, Ishihara KN. Economies of scale in ammonia synthesis loops embedded with iron- and ruthenium-based catalysts. Int J Hydrogen Energy 2021. https://doi.org/10.1016/j.ijhydene.2020.12.081.

[26] Mencarelli L, Chen Q, Pagot A, Grossmann IE. A review on superstructure optimization approaches in process system engineering. Comput Chem Eng 2020;136:1–15. https://doi.org/10.1016/j.compchemeng.2020.106808.

[27] Yeomans H, Grossmann IE. A systematic modeling framework of superstructure optimization in process synthesis. Comput Chem Eng 1999;23:709–31. https://doi.org/10.1016/S0098-1354(99)00003-4.

[28] Smith EMB, Pantelides CC. Design of reaction/separation networks using detailed models. Comput Chem Eng 1995;19.

[29] Zhao Q, Neveux T, Mecheri M, Privat R, Guittard P, Jaubert JN. Superstructure optimization (MINLP) within ProSimPlus Simulator. vol. 43. Elsevier Masson SAS; 2018. https://doi.org/10.1016/B978-0-444-64235-6.50135-2.

[30] ProSim S.A. ProSimPlus - Continuous steady-state process simulator 2020. https://www.prosim.net/en/ (accessed April 4, 2021).

[31] Zhao Q. Conception and optimization of supercritical CO2 Brayton cycles for coal-fired power plant application 2018. https://hal.univ-lorraine.fr/tel-01920767 (accessed April 14, 2021).

[32] Uebbing J, Rihko-Struckmann L, Sager S, Sundmacher K. CO2 methanation process synthesis by superstructure optimization. J CO2 Util 2020;40:101228. https://doi.org/10.1016/j.jcou.2020.101228.

[33] Schlüter M, Egea JA, Banga JR. Extended ant colony optimization for non-convex mixed integer nonlinear programming. Comput Oper Res 2009;36:2217–29. https://doi.org/10.1016/j.cor.2008.08.015.

[34] Schlüter M, Gerdts M. The oracle penalty method. J Glob Optim 2010;47:293–325. https://doi.org/10.1007/s10898-009-9477-0.

[35] Schlueter M, Erb SO, Gerdts M, Kemble S, Rückmann JJ. MIDACO on MINLP space applications. Adv Sp Res 2013;51:1116–31. https://doi.org/10.1016/j.asr.2012.11.006.

[36] Rehberg M, Ritter JB, Genzel Y, Flockerzi D, Reichl U. The relation between growth phases, cell volume changes and metabolism of adherent cells during cultivation. J Biotechnol 2013;164:489–99. https://doi.org/10.1016/j.jbiotec.2013.01.018.

[37] Brodrick PG, Brandt AR, Durlofsky LJ. Optimal design and operation of integrated solar combined cycles under emissions intensity constraints. Appl Energy 2018;226:979–90. https://doi.org/10.1016/j.apenergy.2018.06.052.

[38] Teichgraeber H, Brodrick PG, Brandt AR. Optimal design and operations of a flexible oxyfuel natural gas plant. Energy 2017;141:506–18. https://doi.org/10.1016/j.energy.2017.09.087.

[39] Schlüter M. MIDACO Solver, User Manual 2018. http://www.midaco-solver.com/data/other/MIDACO_User_Manual.pdf (accessed February 4, 2021).

[40] Rouwenhorst KHR, Van der Ham AGJ, Mul G, Kersten SRA. Islanded ammonia power systems: Technology review & conceptual process design. Renew Sustain Energy Rev 2019;114. https://doi.org/10.1016/j.rser.2019.109339.

[41] Sedaghat A, Mostafaeipour A, Rezaei M, Jahangiri M, Mehrabi A. A new semi-empirical wind turbine capacity factor for maximizing annual electricity and hydrogen production. Int J Hydrogen Energy 2020;45:15888–903. https://doi.org/10.1016/j.ijhydene.2020.04.028.

[42] López-Paniagua I, Rodríguez-Martín J, Sánchez-Orgaz S, Roncal-Casano JJ. Step by step derivation of the optimum multistage compression ratio and an application case. Entropy 2020;22:1–13. https://doi.org/10.3390/E22060678.

[43] Khademi MH, Sabbaghi RS. Comparison between three types of ammonia synthesis reactor configurations in terms of cooling methods. Chem Eng Res Des 2017;128:306–17. https://doi.org/10.1016/j.cherd.2017.10.021.

[44] Nielsen A, Kjaer J, Hansen B. Rate equation and mechanism of ammonia synthesis at industrial conditions. J Catal 1964;3:68–79. https://doi.org/10.1016/0021-9517(64)90094-6.

[45] Palys M, McCormick A, Cussler E, Daoutidis P. Modeling and Optimal Design of Absorbent Enhanced Ammonia Synthesis. Processes 2018;6:91. https://doi.org/10.3390/pr6070091.

[46] Rossetti I, Pernicone N, Ferrero F, Forni L. Kinetic study of ammonia synthesis on a promoted Ru/C catalyst. Ind Eng Chem Res 2006;45:4150–5. https://doi.org/10.1021/ie051398g.

[47] Privat R, Jaubert JN, Mutelet F. Use of the PPR78 model to predict new equilibrium data of binary systems involving hydrocarbons and nitrogen. Comparison with other GCEOS. Ind Eng Chem Res 2008;47:7483–9. https://doi.org/10.1021/ie800636h.

[48] Chauvel A, Fournier G, Raimbault C. Manual of Process Economic Evaluation. Paris: Editions Technip; 2003.

[49] Peduzzi E, Boissonnet G, Haarlemmer G, Maréchal F. Thermo-economic analysis and multi-objective optimisation of lignocellulosic biomass conversion to Fischer-Tropsch fuels. Sustain Energy Fuels 2018;2:1069–84. https://doi.org/10.1039/c7se00468k.